NIH Public Access
Author Manuscript
Biomaterials. Author manuscript; available in PMC 2013 March 19.

Published in final edited form as:
Biomaterials. 2011 October ; 32(30): 7432–7443. doi:10.1016/j.biomaterials.2011.06.027.

The effect of vascular endothelial growth factor (VEGF) presentation within fibrin matrices on endothelial cell branching

Sean M. Anderson, **Shayne N. Siegman**, and **Tatiana Segura***
University of California, Los Angeles, Chemical and Biomolecular Engineering Department, Los Angeles, CA

Introduction

Tissue regeneration involves the growth of specific tissue types for replacement of damaged tissue that the body is incapable of regenerating[1]. In order to assimilate the new tissue implant into the body and to support survival of the growing cells within the implant, a vascular supply is typically required[2]. Infiltration of blood vessels into the implant, however, is not enough to guarantee adequate blood supply, nutrient delivery, and waste removal for the cells inhabiting the implant. To maintain the integrity of the new tissue, perfusion of the implant by branched capillaries is needed to provide a feasible infrastructure upon which the new tissue can mature[3].

Research over the past two decades has led to the development of biomaterials that support vascular formation within a tissue implant. Encapsulation of growth factors that rely on non-specific release and diffusion to the target receptors is one method of supplementing a biomaterial scaffold with cell instructive molecules[4-6]. A more sophisticated method involves covalent incorporation of growth factors with genetically engineered domains that allow release upon secretion of proteases by migrating cells participating in natural wound healing—a method termed cell demanded release[7, 8]. Electrostatic binding of VEGF to synthetic and natural polymers including PLGA and heparin can extend the release kinetics of the growth factor[9-12]. Instead of distributing these VEGF-binding polymers homogeneously throughout the matrix, VEGF can be sequestered to particles composed of these polymers leading to heterogeneity within the matrix[13].

VEGF has also been covalently bound to the polymer backbone of a biomaterial without an engineered release mechanism. However, a natural release mechanism is found in VEGF-165 between the receptor binding domain and the extracellular matrix binding domain[14]. A ten amino acid sequence located in this region can be cleaved by specific matrix metalloproteinases secreted into the environment by infiltrating endothelial cells[15]. Binding VEGF in this fashion has led to formation of branched, stable vessel structures capable of perfusion[16, 17].

In this present report, we are interested in understanding the role of VEGF presentation on vessel branching. To study the role of growth factor presentation on branching, we established a system in which VEGF is bound with increasing affinity for the matrix, and in increasing heterogeneity with respect to its distribution in the gel. Polystyrene particles 260 nm in diameter were coated with heparin which was modified with a photoactive crosslinker. VEGF is covalently bound to the particle in a bind-and-lock approach[18]. To vary the affinity of VEGF for the matrix from covalent to electrostatic, the photoactive

*Corresponding author: Tatiana Segura 420 Westwood Plaza 5531 Boelter Hall Los Angeles, CA 90095, tsegura@ucla.edu.

NIH-PA Author Manuscript
NIH-PA Author Manuscript
NIH-PA Author Manuscript

NIH-PA Author Manuscript

NIH-PA Author Manuscript

NIH-PA Author Manuscript

crosslinker is omitted. To modify the distribution of the growth factor in the gel, VEGF is bound in low density and high density forms, where the low density form has less VEGF molecules bound per particle. By maintaining a constant growth factor concentration between the conditions, the low density form represents a more homogenous distribution of the growth factor in the gel. The particles were characterized for binding, release kinetics, and activity, both on a cellular level and a molecular level. The particles were embedded into a fibrin gel and combined with HUVECs in a tube formation assay [19] to study the effect of VEGF presentation on tube branching. Finally, the particle-fibrin gels are introduced to the CAM of a chicken embryo and assayed for angiogenic potential. In addition to the polystyrene particles, heparin nanoparticles composed of a modified heparin polymer are bound to VEGF in the same approach and analyzed concurrently. The particles offer an alternative approach to the polystyrene particles for use in future investigations into *in vivo* applications.

Materials and Methods

Materials

Heparin sodium salt from porcine intestinal mucosa was purchased from Alfa Aesar (Ward Hill, MA). Vascular Endothelial Growth Factor (VEGF) was kindly provided by the National Cancer Institute. Human umbilical vein endothelial cells (HUVEC) were purchased from Lonza (Walkersville, MD). Polystyrene particles were purchased from Spherotech (Lake Forest, IL). Fibrinogen was purchased from Enzyme Research Laboratories (South Bend, IN). Cytodex beads were purchased from Sigma-Aldrich (St. Louis, MO). Fertilized eggs were purchased from Kendor farms (Lake Balboa, CA). All other reagents and products were purchased from Fisher Scientific unless noted otherwise.

Cell culture

HUVECs were cultured in EGM-2 complete medium (Lonza, Walkersville, MD) at 37°C and 5% CO_2. The HUVECs were first obtained and cultured to passage 2. Tube formation experiments were conducted while the cells were at passage 2. In order to provide enough cells for all of the other experiments, the cells were expanded and frozen at passage 7. For each experiment, the cells were thawed and grown for 2 days in a T75 flask (Corning, Corning, NY), before being plated onto a 6 well dish. Fibroblast cells were a kind gift from Dr. Arispe, and these cells were cultured in EGM-2 complete medium.

Heparin polystyrene coated nanoparticle preparation

Heparin was oxidized by dissolving 62.5 mg/ml heparin in 200 mM sodium periodate in 100 mM sodium acetate pH 4 for 30-60 minutes. The reaction was quenched with addition of glycerol, then diluted to 3 mg/ml heparin and adjusted to pH 7 with PBS. Heparin became photoactive by addition of azido-benzyl hydrazide (ABH, Pierce, Rockford, IL) for 2 hours at room temperature. The solution was then diluted to 1 mg/ml heparin and adjusted to pH 9-9.5 before incubating with amine functionalized polystyrene particles 260 nm in diameter for 2 hours at room temperature. Then, the particles were incubated with 50 mM sodium cyanoborohydride for 5 minutes at room temperature. The amount of polystyrene particles in the solution was determined by the following relation using information provided by the manufacturer (from Spherotech Technical Notes):

$$N=\frac{6W}{\pi PD^3}\times 10^{12}$$

NIH-PA Author Manuscript

NIH-PA Author Manuscript

NIH-PA Author Manuscript

where N is the number of particles, W is the weight of the polymer (g), P is the density of the polymer (g/cm^3), and D is the diameter (μm). Overnight incubation of VEGF at 4°C in 1% BSA-PBS at 100 μg/ml was followed by 365 nm wavelength UV light activation for 10 minutes to lock VEGF covalently to the surface. Excess VEGF was removed by dialysis in 100 kD MWCO dialysis units.

Heparin nanoparticle synthesis

Heparin was first modified with p-azidobenzyl hydrazide (ABH, Pierce, Rockford, IL) through EDC mediated conjugation in a 1:3 molar ratio of ABH to available carboxylic acids. The pH was monitored during the course of the reaction and the conjugation took place at pH 4.75 in PBS. After 2 hours of reaction at room temperature, the carboxylic acid groups on heparin were reactivated with EDC, but this time reacted with adipic dihydrazide (ADH) in 27 molar excess in order to saturate reaction binding sites and prevent unwanted crosslinking. Again, the reaction pH was monitored at pH 4.75 in PBS. This reaction was allowed to proceed overnight at room temperature, at which point the reaction solution was dialyzed against DI water. The dialysis units were then placed in PBS at pH 7.4 for buffer exchange. Heparin with ABH and ADH was then reacted with NHS-acrylate to convert the amine groups to acrylates. The reaction proceeded overnight at room temperature, and then dialyzed again. After dialysis, the solution was lyophilized for two days. The powder was dissolved in sodium acetate, pH 4, at 100 mg/ml and combined with Tween-80 and Span-80 (8% HLB). The solution was placed in a ten-fold volume of hexane and combined with *N,N,N',N'*-tetramethyl-ethane-1,2-diamine (TEMED) and ammonium persulfate (APS) during sonication to initiate radical polymerization. The resultant nanoparticles were purified via liquid-liquid extraction in hexane. In the final stage of the extraction process, bubbling nitrogen gas into the nanoparticle solution evaporated off excess hexane. The particles were then dialyzed in 100 kD MWCO dialysis units for several days and stored until use. The amount of heparin in the solution was determined by lyophilizing a small aliquot of the solution. Similar to the heparin-coated polystyrene particles, VEGF was incubated at 4°C at 100 μg/ml, followed by 365 nm wavelength UV light activation for 10 minutes to lock VEGF covalently to the surface. Excess VEGF was removed by dialysis in 100 kD MWCO dialysis units.

Dynamic light scattering (DLS)

Heparin-polystyrene coated nanoparticles were analyzed in a Malvern Zetasizer to determine particle diameter after each preparation step. Heparin nanoparticles were analyzed after formation, purification, and dialysis. Samples were loaded into a filtered DI water cleaned quartz cuvette. Ten runs each comprised three measurements, and data was reported as Z-average with polydispersity index (PDI).

Enzyme linked immunosorbant assay (ELISA)

Following dialysis, nanoparticles were collected and quantified for amount VEGF bound using the human VEGF Duoset from R&D Systems (Minneapolis, Minnesota) following manufacturer's instructions. Briefly, the plate was coated with "capture" antibody overnight at room temperature, then non-specific binding sites were blocked via incubation with 1% BSA in PBS. The samples were added for 2 hours at room temperature with gentile agitation. The plates were washed several times, and "detection" antibody probed the 96-well plate for presence of VEGF. Streptavidin-HRP diluted 1:200 in 1% BSA-PBS was then incubated with the wells for 20 minutes. TMB substrate (Cell Signaling, Boston, MA) was added to the wells for 20 minutes at room temperature, and then read at 645 nm with 570 nm correction.

NIH-PA Author Manuscript

NIH-PA Author Manuscript

NIH-PA Author Manuscript

Cell migration

HUVECs were grown to confluency in a 6 well plate and then scratched with a pipet tip to create a wound. Phase micrographs captured the initial size of the wound created by the pipet tip for each condition. Soluble VEGF or VEGF nanoparticles at 2 ng/ml were added to the wells. After 18 hours, phase micrographs were taken again. ImageJ software was used to quantify the percent wound closure for each condition. Photographs were acquired using a Zeiss Observer microscope.

VEGFR-2 phosphorylation assay

HUVECs were grown to confluency in a 6 well plate, and then serum starved for 6 hours. Prior to growth factor treatment, the cells were treated with 0.1 mM sodium vanadate for 5 minutes. The cells were then treated with 2 ng/ml of either soluble or bound VEGF at 37°C for 5 minutes. The cells were rinsed twice with ice cold PBS supplemented with 0.2 mM sodium vanadate. After aspirating all remnants of liquid from the wells, 100 μl of lysis buffer (1% Non-idet, 10 mM Tris-HCl, pH 7.6, 150 mM NaCl, 30 mM sodium pyrophosphate, 50 mM sodium fluoride, 2.1 mM sodium orthovanadate, 1 mM EDTA, 1 mM phenylmethylsulfonyl fluoride, and 2 μg/ml of aprotinin) was added to the surface and scraped. Insoluble cell material was removed by centrifugation at 4°C for 10 min at 14,000 rpm (Beckman Coulter Microcentrifuge 22R). Equal amounts of cell lysate (BCA assay, Bio-Rad) were diluted in 5X loading buffer (1 M Tris-HCL, pH 6.8, 20% SDS, 50% glycerol) supplemented with 5% (v/v) ß-mercaptoethanol, boiled for 10 min at 70°C, separated by SDS-PAGE (8% resolving, 2 h at 130 V), and transferred to nitrocellulose membranes (2 h at 400 mA). The membranes were incubated in blocking buffer (5% milk in 0.1% Tween-20 in TBS) for 1 h at room temperature before overnight incubation with primary antibodies. Phosphorylated proteins were detected by immunoblotting using anti-phosphotyrosine antibodies (pVEGFR-2/1175 Cell Signaling, pVEGFR-2/1214 Invitrogen, in blocking buffer) followed by secondary antibodies coupled with horseradish peroxidase (200 ng/ml, Invitrogen, 1 h at room temperature) and visualized by chemifluorescence (ECL detection reagents, GE Healthcare) using a Typhoon scanner (GE, Amersham Biosciences). Protein-loading control was assessed by Western blot using anti-VEGFR-2 (Cell Signaling Technology). Typhoon images were analyzed and normalized with ImageJ software.

Cdc42 GLISA

Cells were treated for 5 minutes following the same method mentioned earlier. After treatment, the cells were lysed and quantified with ProteinRed. The samples were assayed with the CytoSkeleton (Denver, CO) cdc42 GLISA kit following manufacturer's instructions. Samples were loaded at 0.5 mg/ml, and absorbance read at 490 nm.

Tube formation assay and quantification

HUVECs were grown in a T25 flask until confluency. Meanwhile, cytodex beads were autoclaved and then coated with fibronectin (Millipore, Temecula, CA) in an incubation solution of 10 μg/ml at 37°C for 2 hours. The cells were trypsinized and combined with the cytodex beads at a ratio of 1 million cells per 1200 beads for 4 hours at 37°C with occasional agitation. The HUVEC-coated cytodex beads were cultured overnight in a T25 flask, and then combined in the pre-gel solution at a concentration of 500 beads/ml. Fibrinogen was diluted from its stock to 2 mg/ml and supplemented with aprotinin. VEGF nanoparticles at 200 ng/ml were combined with the fibrinogen and cytodex bead/HUVEC solution. Fibrin gel formation was initiated by adding 1.25 U/ml of thrombin in a 10% v/v ratio. The gels were allowed to stand for 5 minutes at room temperature, and then incubated at 37°C for 15 minutes. Meanwhile, fibroblast cells were trypsinized and plated at 40,000 cells/condition. The cells were cultured in VEGF withdrawn EGM-2 media for 9 days. The

NIH-PA Author Manuscript

NIH-PA Author Manuscript

NIH-PA Author Manuscript

soluble VEGF condition was refreshed every other day with new soluble VEGF (200 ng/ml). Phase micrographs captured the tube formation, and quantification was completed in ImageJ. For each condition, 10 beads were analyzed. Branching points were considered where two tubes grew out of a single tube. Sprouts were measured as tubes originating from the cytodex bead. Total network length was calculated by measuring the distance from the bead to the end of the sprout, and summing for all the sprouts on the bead. Thickness was measured across the vessel away from its base (interface with the bead).

Chorioallantoic membrane assay (CAM)

Fertilized eggs were purchased from Kendor farms (Lake Balboa, CA) and stored in a humidified chamber for 2 days at 38°C. Air was released from the egg to flatten the embryo by inserting the tip of a 32 ½ gauge needle into the broad side of the egg. After 2 additional hours of storage in the chamber, the eggs were opened and the embryo was transferred into a petri dish. The embryos continued to grow in the petri dishes within a humidified incubator at 38°C for 6 days. Fibrin gels were prepared as previously mentioned, with the exception of cytodex bead incorporation, and a VEGF dosage increase to 2 μg/ml. The fibrin gels were grafted onto regions of the CAM located at a distance from the embryo and major vessels. After 2 days of incubation in the incubator, the vessels were perfused with FITC-dextran and allowed to circulate for 5 minutes. The gels and CAM surrounding the gels were removed and fixed in 4% paraformaldehyde. The embryos were then sacrificed. Micrographs were captured on a small Zeiss microscope. The fluorescent images were captured on a Zeis Observer using the 488 nm filter. The fibrin gel and the area surrounding the fibrin gel were photographed in order to determine the presence of vessels within the implant, and the morphology of vessels surrounding the implant.

Statistical analysis

Data are presented as mean ± standard deviation. To identify significant trends in data, statistical comparisons were performed by one-way ANOVA with post-test using the Tukey method. Data were considered significantly different if $p < 0.05$.

Results

Heparin-coated polystyrene and heparin nanoparticle synthesis

To understand the role of VEGF presentation on branching morphogenesis in biomaterials, polystyrene nanoparticles 260 nm in diameter were coated with oxidized heparin as outlined in Figure 1. Heparin underwent periodate-mediated oxidation and conjugation to p-azidobenzyl hydrazide (ABH). The reaction was done in excess of aldehyde groups to ensure remaining binding sites for conjugation to amine-functionalized polystyrene particles. After reducing the Schiff base with sodium cyanoborohydride, the particles were washed several times, and then incubated with VEGF. Upon exposure to UV light, the VEGF became covalently bound to the polystyrene particle (Figure 1)[18].

Nanoparticles composed of only heparin were also developed using an inverse emulsion process. Heparin was modified via EDC/NHS chemistry to introduce photoreactive and acrylate functionalities. First, ABH was reacted in excess of carboxylic acid groups to ensure remaining binding sites for the next conjugation step. Then, adipic dihydrazide (ADH) was incubated with heparin in large molar excess to ensure efficient conjugation to the remaining carboxylic acid groups and reduce the occurrence of unintended crosslinking. Next, N-acryloxysuccinimide (NHS-acrylate) was conjugated to the hydrazide groups. The polymer solution was then added to a ten-fold volume of hexane with surfactants Tween-80 and Span-80, and sonicated with addition of radical initiators *N,N,N',N'*-tetramethyl-ethane-1,2-diamine (TEMED) and ammonium persulfate (APS). The heparin nanoparticles

NIH-PA Author Manuscript

NIH-PA Author Manuscript

NIH-PA Author Manuscript

formed from this radical polymerization in the template of the nanoemulsion generated during the sonication treatment. Similar to the polystyrene particles, the heparin nanoparticles were incubated with VEGF, and then exposed to UV light to induce covalent attachment of the growth factor to the nanoparticle (Figure 1).

Dynamic light scattering (DLS) measurements confirmed modification of the polystyrene particles, with significant increases in diameter from heparin coating and VEGF loading (Figure 2A). As expected, with the addition of each layer, the PDI increased from below 0.1 to 0.2. For the heparin nanoparticles, DLS measurements indicated that the Z-average size was 58.36 ± 0.42 nm, with a PDI of 0.46 (Figure 2B).

VEGF nanoparticle loading characterization

VEGF was loaded onto the heparin-coated polystyrene particles and then monitored over several days to characterize the release kinetics of the growth factor from the nanoparticles. As a control, heparin-coated polystyrene without the photoactive crosslinker, and polystyrene particles without heparin were included in the analysis. Release of covalently bound VEGF was significantly less than that released from heparin-coated particles without the photoactive crosslinker and un-coated polystyrene particles (Figure 3A). Direct binding of VEGF to the heparin-coated polystyrene particles was investigated next for high binding and low binding densities. After converting the ELISA readings to molecules of VEGF, and calculating the number of particles, the data was presented as VEGF molecules per particle. For both the covalent and electrostatic binding conditions, the high binding density was 1000 VEGF molecules per particle and the low binding density was 200 VEGF molecules per particle (Figure 3B). For later experiments, these solutions were normalized to equivalent VEGF concentrations.

The heparin nanoparticles were washed and the washes were analyzed for VEGF content. With each successive wash, the amount of VEGF decreased until remaining steady (Figure 3C). After these washes, the heparin nanoparticles were analyzed for VEGF content, and the amount was normalized to mg of heparin to show high binding and low binding densities. The high binding heparin nanoparticle had 23 μg VEGF/mg heparin while the low binding heparin nanoparticle had 10 μg VEGF/mg heparin (Figure 3C). Again, the VEGF nanoparticle solutions were equalized relative to VEGF concentration before use in the subsequent experiments.

Wound closure and VEGFR-2 phosphorylation studies

To test the activity of VEGF modified nanoparticles, *in vitro* wound closure, VEGFR-2 phosphorylation, and cdc42 activation were studied. A scratch was introduced to a confluent monolayer of human umbilical vein endothelial cells (HUVECs) and VEGF coated nanoparticles were incubated with the cells at a VEGF concentration of 2 ng/ml for all conditions. The closure of the wound was monitored over 18 hours and the percent wound closure was quantified (Figure 4A). VEGF covalently bound to both polystyrene and heparin particles led to wound closure rates comparable to the soluble VEGF control (Figure 4B).

VEGF modified nanoparticles were able to phosphorylate VEGFR-2 at two different tyrosine residues, Y1175 and Y1214 (Figure 5). Interestingly, the intensity of receptor phosphorylation was different between Y1175 and Y1214 for cells exposed to soluble or VEGF coated particles, with Y1175 being more phosphorylated relative to Y1214 when cells were exposed to soluble VEGF and Y1214 being more phosphorylated relative to Y1175 when cells were exposed to VEGF coated nanoparticles.

We next tested the levels of cdc42 when the cells were presented with the particle-bound VEGF. We observed a statistically significant increase in cdc42 activation for VEGF

NIH-PA Author Manuscript

NIH-PA Author Manuscript

NIH-PA Author Manuscript

modified heparin nanoparticles at high (hNP_{high}) surface concentration compared to soluble VEGF (Vs) presentation ($p < 0.05$, Figure 6). Although there was activation of cdc42 with the polystyrene modified particles at high and low density and for both covalent (PS-$Vc_{high/low}$) and electrostatically (PS-$Ve_{high/low}$) immobilized VEGF, there was no statistical significance between any of the polystyrene modified VEGF particles and Vs ($p > 0.05$).

Effect of VEGF presentation inside fibrin hydrogels on HUVEC morphology

To determine the effect of VEGF presentation on endothelial tube formation, a sprouting bead assay was used in which cytodex beads are coated with endothelial cells and the beads are placed inside a fibrin hydrogel scaffold, while fibroblast cells are seeded on top of the hydrogel (Figure 7-8A)[19, 20]. During fibrin hydrogel formation either 200 ng/ml VEGF modified nanoparticles, unmodified nanoparticles, or 200 ng/ml soluble VEGF were encapsulated within the hydrogel. The HUVEC tubes from the cytodex beads were then quantified for branching points, sprouts, thickness, and total vessel network length (Figure 1D, Figure 7-8).

The number of branching points for PS-Vc_{high} and PS-Ve_{high} was statistically higher than for that observed for Vs ($p <$ at least 0.01, Figure 7B). However, lowering the amount of VEGF displayed per particle, PS-Vc_{low} and PS-Ve_{low}, resulted in no significant increase in branching over Vs ($p > 0.05$), indicating that the presentation of the VEGF inside the fibrin hydrogel affected the architecture of the vessels formed. Comparing between PS-Vc_{high} vs. PS-Vc_{low} and PS-Ve_{high} vs. PS-Ve_{low} there was a statistically significant difference for PS-Vc ($p < 0.001$) but not for PS-Ve ($p > 0.05$), further indicating that the presentation of VEGF affected branching. No difference was observed between PS-Vc_{high} and PS-Ve_{high} ($p > 0.05$).

The total network length was quantified by measuring the length of individual sprouts and then summing for each bead (Figure 7C). The total network length for PS-Vc_{high} and PS-Ve_{high} was statistically higher than for that observed for Vs ($p < 0.001$). However, lowering the amount of VEGF displayed per particle, PS-Vc_{low} and PS-Ve_{low}, resulted in no significant increase in network length over Vs for PS-Vc_{low} ($p > 0.05$) and a statistically significant increase in network length for PS-Ve_{low} ($p < 0.001$), indicating that the presentation of the VEGF inside the fibrin hydrogel modulated the extent of the vascular network formed. Comparing between PS-Vc_{high} vs. PS-Vc_{low} and PS-Ve_{high} vs. PS-Ve_{low} there was a statistically significant difference for PS-Vc ($p < 0.001$) but not for the PS-Ve ($p > 0.05$), further indicating that the presentation of VEGF affected the extent of the network. No difference was observed between PS-Vc_{high} and PS-Ve_{high} ($p > 0.05$).

Next, the number of sprouts from the cytodex bead and tube thickness were quantified. No differences were observed for any of the particles tested compared to Vs (Figure 7D,E), indicating that the induction of angiogenesis was not dependent on VEGF presentation nor was the thickness of the vessel formed.

Since no major differences between covalent and electrostatically bound VEGF were observed, when we sought to translate the PS particles to a more biocompatible particle, only covalently bound VEGF was used. VEGF modified heparin nanoparticles were synthesized and similar analysis as those done with PS nanoparticles were performed (Figure 8). Similarly to the VEGF modified PS nanoparticles, the number of branching points for hNP_{high} was statistically significantly higher from the number of branching points observed in Vs ($p < 0.001$) and the number of branching points for hNP_{low} was not statistically significant from Vs ($p > 0.05$, Figure 8B). These findings further pointed to the role of VEGF presentation on endothelial cell branching. Comparing between hNP_{high} and hNP_{low} showed statistically higher branching for hNP_{high} ($p < 0.01$, Figure 8B). To

NIH-PA Author Manuscript

NIH-PA Author Manuscript

NIH-PA Author Manuscript

determine if the preloading of VEGF to the nanoparticles was necessary or the presence of the heparin nanoparticles alone was sufficient to recruit soluble VEGF into nanodomains, unloaded heparin nanoparticles were introduced to the hydrogel. A statistically higher number of branching points were observed for the hydrogels that contained unloaded nanoparticles along with soluble VEGF (VS-hNP) than those with only Vs ($p < 0.05$). This data indicated that the presence of the nanoparticles alone was sufficient to recruit VEGF into clusters that changed the growing vessel architecture.

Similar to that observed with the VEGF modified polystyrene nanoparticles, total network length for hNP_{high} and hNP_{low} was statistically higher than that observed for Vs ($p < 0.001$, Figure 8C), further suggesting the presentation of VEGF affected the extent of the vessel network. However, as was the case for the VEGF coated PS nanoparticles, the binding density on hNP did not result in a statistical difference for hNP_{high} and hNP_{low}. Pre-loading of hNP with VEGF did result in a significant difference between hNP_{high} ($p < 0.05$) and Vs-hNP, but not hNP_{low} and Vs-hNP. The presence of hNP alone with Vs led to a significant increase in vessel network formation for Vs-hNP v. Vs ($p < 0.001$).

Similar to PS, hNP did not change the number of sprouts to a significant extent over Vs (Figure 8D). One difference between VEGF modified PS nanoparticles and hNP was that tube thickness for hNP_{high} and Vs-hNP was significantly higher compared to Vs (Figure 8E). No other differences were observed between the conditions.

VEGF nanoparticles in fibrin gels on CAM

Fibrin gels with VEGF nanoparticles were placed on the chorioallantoic membrane (CAM) of embryonic chicken. After two days, the implants were removed and analyzed for induction of angiogenesis (Figure 9). The presence of VEGF had a noticeable increase in blood vessel density surrounding the implant. VEGF release from the implants was noted by the appearance of radial blood vessels originating from the fibrin gel protruding outward.

To further study the extent of vessel induction and infiltration into the implant, the embryo was perfused with FITC-Dextran. In $PS\text{-}Vc_{high}$ and hNP_{high}, microvessels inside the fibrin implant were observed, indicating that not only were vessels inside the implant formed, but that the vessels were integrated with the host vasculature (Figure 10). The PS-Ve gel did not facilitate infiltration of blood vessels into the fibrin gel. However, there were radial blood vessels originating from the gel, indicating that the VEGF was released from the particles and diffused out of the gel. The Vs fibrin gel also did not show blood vessel formation in the fibrin gel, but did show characteristic radial vessel formation outside of the gel (Figure 10).

Discussion

Vascular endothelial growth factor (VEGF) has been extensively investigated to promote vascularization at damaged or diseased sites and in tissue implants for tissue engineering applications[21]. In this current report, we studied if the manner in which VEGF is presented from a scaffold to endothelial cells influences the architecture of the blood vessels formed. We bound VEGF to nanoparticles and placed these nanoparticles inside fibrin hydrogels, which contained HUVECs bound to cytodex beads. Fibroblast cells are plated on top of the fibrin gel to further mimic a physiologic environment[20]. We tested VEGF bound electrostatically or covalently and in high density and low density formats to study differences between growth factor presentation in heterogeneous nanodomains and homogenous distribution. We found that VEGF covalently bound to nanoparticles at high density led to increases in HUVEC tube branching, thickness, and total vessel network length compared to soluble VEGF. Our data indicates that the presentation of VEGF within matrices determines the architecture of the resulting blood vessels.

NIH-PA Author Manuscript

NIH-PA Author Manuscript

NIH-PA Author Manuscript

VEGF modified nanoparticles were synthesized using either a polystyrene core (PS) or a heparin core. For the PS nanoparticles the surface of the nanoparticles contained amines, which were used to immobilize heparin. To immobilize VEGF covalently or electrostatically to the PS-heparin particle surface we used either heparin modified with a photoreactive group or unmodified heparin as we have previously described[18]. For the nanoparticles that contained a heparin core, heparin nanoparticles were first generated using an inverse emulsion of water in hexane[22]. The heparin was modified with the same photoreactive group used above to covalently bind VEGF to the surface of the nanoparticle.

The first variable, matrix affinity, was modulated by inclusion of a photoactive crosslinker during nanoparticle synthesis. The release kinetics show that when VEGF is covalently bound to the nanoparticle, less release over time is observed, indicating that the covalent bond reduces the release of VEGF from the nanoparticle (Figure 3). The second variable, distribution, was controlled by incubating VEGF with different amounts of particles. The result is particles with different binding densities of VEGF. In order to normalize the amount of VEGF supplied to the cells during the analysis, more particles with low VEGF binding density are required. This leads to a situation where the growth factor is more homogeneously distributed throughout the gel relative to the high binding condition. The control for both matrix affinity and distribution is soluble VEGF. It is provided freely diffusible during hydrogel formation and in the media changes.

To determine if the process of immobilization affects VEGF activity, HUVEC migration and VEGFR-2 phosphorylation induced by VEGF modified nanoparticles or soluble VEGF were compared. The migration rates are comparable to the soluble treatment (Figure 4), indicating that the VEGF remains active throughout the process of particle modification. At the molecular level, VEGFR-2 phosphorylation at two sites, Y1175 and Y1214, was investigated to ensure that the immobilized VEGF could phosphorylate its receptor. Covalently bound VEGF to nanoparticles appears to enhance activation of Y1214 compared to the soluble condition (Figure 5). Interestingly, the same is observed for VEGF bound to bulk matrices where bound VEGF results in enhanced Y1214 phosphorylation over that observed with Vs [23](Anderson et al, *submitted*). The particles appear to be slightly less effective in activation of Y1175. Phosphorylation at Y1175 results in the activation of the Akt pathway and cellular proliferation[24-26], while phosphorylation at Y1214 results in the activation of the p38 pathway and cellular migration[27, 28]. In addition phosphorylation at Y1214 leads to the activation of cdc42 [27], which is involved in branching. To determine if VEGF modified nanoparticles result in activation of cdc42, a GLISA assay was performed. Heparin nanoparticles modified with VEGF at high density were the most effective in activating cdc42 (Figure 6). As mentioned, this GTPase is directly involved with processes at the cell membrane that lead to filopodia formation[29], which eventually result in branching orchestrated by the leading tip cell[30-32].

The trends observed in the *in vitro* tube formation studies highlight the importance of pre-loading of VEGF for hNP and high density binding. Interestingly, Vs-hNP had significantly more branching than Vs ($p < 0.05$), indicating that the presence of hNP alone with Vs was able to affect change in branching behavior. However, pre-loading of VEGF onto hNP in high density significantly increased branching over Vs-hNP ($p < 0.01$). Vs-hNP also led to a larger vessel network with thicker vessels, but still was not as efficient at inducing more network size as pre-loaded hNP in high density. By binding VEGF to nanoparticles in the high binding density format, growth factor reservoirs are created, mimicking the physiological environment[33-35]. Growth factors in the extracellular matrix (ECM) are not homogeneously dispersed, but rather clustered into these reservoirs. While the high density binding of VEGF does not lead to a larger network compared to low density binding (except

NIH-PA Author Manuscript

NIH-PA Author Manuscript

NIH-PA Author Manuscript

for PS-Vc), it does induce more branching (except PS-Ve). Branching of endothelial tubes is important in creating a capillary network capable of perfusion in the new tissue implant[3].

Covalently binding VEGF does not allow VEGF to easily release and diffuse out of the gel. Electrostatic binding may not be adequate in the complex environment to retain VEGF and facilitate infiltration of the vessels into the matrix (Figure 10). Previous work in our own laboratory has found that when VEGF DNA is delivered to cells, the VEGF that is produced leaves the gel and results in the radial vessel morphology observed in the soluble condition[36]. Production of VEGF in the gel does not guarantee it is retained within the gel. Covalently bound VEGF can release via action by MMP's[15], but the advantage of covalent binding can be seen in the CAM assay where blood vessel infiltration is observed. Electrostatically binding VEGF is secure in a non-competitive environment, but in a complex solution other molecules with affinity for heparin can displace the bound VEGF, releasing it[18].

The high density and low density binding conditions did not show much difference at the molecular level, but did show observable differences in the tube formation experiment and the CAM assay. Further, between the high density cases, matrix affinity does not lead to significant changes in the tube branching. The choice to include the covalent bond in the heparin nanoparticles is made based on the evidence generated here that the covalent bond does not hinder VEGF activity or downstream activation, and it has a stabilizing effect, particularly in a biomaterial setting. This serves as a motivation for development of the heparin nanoparticles, since polystyrene is not a biocompatible material[37]. However, in the course of the material characterization, the heparin nanoparticles have been found to be consistently polydisperse. Despite this, no significant negative impact of this polydispersity is observed for high PDI heparin nanoparticles compared to low PDI polystyrene nanoparticles, suggesting that this polydispersity may be tolerable. This evidence suggests that cluster size, specifically, may not affect the morphological behavior of endothelial tubes, but nanoscale clustering in general does increase vascular network size and degree of branching.

Conclusion

Heparin coated polystyrene and heparin derived nanoparticles were covalently conjugated to VEGF through a bind-and-lock approach at different binding densities. The particles were characterized for amount VEGF bound and activity, both at a cellular and molecular level. Increasingly clustered growth factor nanodomains resulted in more endothelial tube branch points than more homogeneously distributed bound growth factor and soluble VEGF. The high density VEGF nanodomains also led to a larger total network length over VEGF presented in the freely diffusible form. When administered to the CAM of an embryonic chicken, the clustered, covalently bound VEGF nanoparticles successfully guided host vasculature into the implant, leading to a perfused capillary network within the fibrin gel.

Acknowledgments

The authors would like to acknowledge the assistance of Talar Tokatlian on the Malvern Zetasizer. Funding for this project was provided by a seed grant from the Jonsson Cancer Comprehensive Center at the University of California, Los Angeles.

References

1. Lanza, RP.; Langer, RS.; Vacanti, J. Principles of tissue engineering. 3rd ed.. Elsevier Academic Press; Boston: 2007.

NIH-PA Author Manuscript NIH-PA Author Manuscript NIH-PA Author Manuscript

2. Novosel EC, Kleinhans C, Kluger PJ. Vascularization is the key challenge in tissue engineering. Adv Drug Deliv Rev. 2011 doi:10.1016/j.addr.2011.03.004.
3. Kannan RY, Salacinski HJ, Sales K, Butler P, Seifalian AM. The roles of tissue engineering and vascularisation in the development of micro-vascular networks: a review. Biomaterials. 2005; 26:1857–75. [PubMed: 15576160]
4. Gu F, Amsden B, Neufeld R. Sustained delivery of vascular endothelial growth factor with alginate beads. J Control Release. 2004; 96:463–72. [PubMed: 15120902]
5. Huang M, Vitharana SN, Peek LJ, Coop T, Berkland C. Polyelectrolyte complexes stabilize and controllably release vascular endothelial growth factor. Biomacromolecules. 2007; 8:1607–14. [PubMed: 17428030]
6. Edelman ER, Mathiowitz E, Langer R, Klagsbrun M. Controlled and modulated release of basic fibroblast growth factor. Biomaterials. 1991; 12:619–26. [PubMed: 1742404]
7. Ehrbar M, Djonov VG, Schnell C, Tschanz SA, Martiny-Baron G, Schenk U, et al. Cell-demanded liberation of VEGF121 from fibrin implants induces local and controlled blood vessel growth. Circ Res. 2004; 94:1124–32. [PubMed: 15044320]
8. Zisch AH, Lutolf MP, Ehrbar M, Raeber GP, Rizzi SC, Davies N, et al. Cell-demanded release of VEGF from synthetic, biointeractive cell ingrowth matrices for vascularized tissue growth. FASEB J. 2003; 17:2260–2. [PubMed: 14563693]
9. Joung YK, Bae JW, Park KD. Controlled release of heparin-binding growth factors using heparin-containing particulate systems for tissue regeneration. Expert Opin Drug Deliv. 2008; 5:1173–84. [PubMed: 18976129]
10. Lee J, Lee KY. Local and sustained vascular endothelial growth factor delivery for angiogenesis using an injectable system. Pharm Res. 2009; 26:1739–44. [PubMed: 19384466]
11. Zieris A, Prokoph S, Levental KR, Welzel PB, Grimmer M, Freudenberg U, et al. FGF-2 and VEGF functionalization of starPEG-heparin hydrogels to modulate biomolecular and physical cues of angiogenesis. Biomaterials. 2010; 31:7985–94. [PubMed: 20674970]
12. King TW, Patrick CW Jr. Development and in vitro characterization of vascular endothelial growth factor (VEGF)-loaded poly(DL-lactic-co-glycolic acid)/poly(ethylene glycol) microspheres using a solid encapsulation/single emulsion/solvent extraction technique. J Biomed Mater Res. 2000; 51:383–90. [PubMed: 10880080]
13. Chung YI, Kim SK, Lee YK, Park SJ, Cho KO, Yuk SH, et al. Efficient revascularization by VEGF administration via heparin-functionalized nanoparticle-fibrin complex. J Control Release. 2010; 143:282–9. [PubMed: 20093158]
14. Fairbrother WJ, Champe MA, Christinger HW, Keyt BA, Starovasnik MA. Solution structure of the heparin-binding domain of vascular endothelial growth factor. Structure. 1998; 6:637–48. [PubMed: 9634701]
15. Lee S, Jilani SM, Nikolova GV, Carpizo D, Iruela-Arispe ML. Processing of VEGF-A by matrix metalloproteinases regulates bioavailability and vascular patterning in tumors. J Cell Biol. 2005; 169:681–91. [PubMed: 15911882]
16. Moon JJ, Saik JE, Poche RA, Leslie-Barbick JE, Lee SH, Smith AA, et al. Biomimetic hydrogels with pro-angiogenic properties. Biomaterials. 2010; 31:3840–47. [PubMed: 20185173]
17. Phelps EA, Landazuri N, Thule PM, Taylor WR, Garcia AJ. Bioartificial matrices for therapeutic vascularization. Proc Natl Acad Sci U S A. 2010; 107:3323–8. [PubMed: 20080569]
18. Anderson SM, Chen TT, Iruela-Arispe ML, Segura T. The phosphorylation of vascular endothelial growth factor receptor-2 (VEGFR-2) by engineered surfaces with electrostatically or covalently immobilized VEGF. Biomaterials. 2009; 30:4618–28. [PubMed: 19540581]
19. Nakatsu MN, Davis J, Hughes CC. Optimized fibrin gel bead assay for the study of angiogenesis. J Vis Exp. 2007; 3:186. [PubMed: 18978935]
20. Nakatsu MN, Sainson RC, Perez-del-Pulgar S, Aoto JN, Aitkenhead M, Taylor KL, et al. VEGF(121) and VEGF(165) regulate blood vessel diameter through vascular endothelial growth factor receptor 2 in an in vitro angiogenesis model. Lab Invest. 2003; 83:1873–85. [PubMed: 14691306]
21. Phelps EA, Garcia AJ. Engineering more than a cell: vascularization strategies in tissue engineering. Curr Opin Biotechnol. 2010; 21:704–9. [PubMed: 20638268]

NIH-PA Author Manuscript

NIH-PA Author Manuscript

NIH-PA Author Manuscript

22. Missirlis D, Tirelli N, Hubbell JA. Amphiphilic hydrogel nanoparticles. Preparation, characterization, and preliminary assessment as new colloidal drug carriers. Langmuir. 2005; 21:2605–13. [PubMed: 15752059]
23. Chen TT, Luque A, Lee S, Anderson SM, Segura T, Iruela-Arispe ML. Anchorage of VEGF to the extracellular matrix conveys differential signaling responses to endothelial cells. J Cell Biol. 2010; 188:595–609. [PubMed: 20176926]
24. Takahashi T, Yamaguchi S, Chida K, Shibuya M. A single autophosphorylation site on KDR/Flk-1 is essential for VEGF-A-dependent activation of PLC-gamma and DNA synthesis in vascular endothelial cells. Embo J. 2001; 20:2768–78. [PubMed: 11387210]
25. Dayanir V, Meyer RD, Lashkari K, Rahimi N. Identification of Tyrosine Residues in Vascular Endothelial Growth Factor Receptor-2/FLK-1 Involved in Activation of Phosphatidylinositol 3-Kinase and Cell Proliferation. J Biol Chem. 2001; 276:17686–92. [PubMed: 11278468]
26. Fujio Y, Walsh K. Akt Mediates Cytoprotection of Endothelial Cells by Vascular Endothelial Growth Factor in an Anchorage-dependent Manner. J Biol Chem. 1999; 274:16349–54. [PubMed: 10347193]
27. Lamalice L, Houle F, Jourdan G, Huot J. Phosphorylation of tyrosine 1214 on VEGFR2 is required for VEGF-induced activation of Cdc42 upstream of SAPK2/p38. Oncogene. 2004; 23:434–45. [PubMed: 14724572]
28. Rousseau S, Houle F, Landry J, Huot J. p38 MAP kinase activation by vascular endothelial growth factor mediates actin reorganization and cell migration in human endothelial cells. Oncogene. 1997; 15:2169–77. [PubMed: 9393975]
29. Mori M, Murata Y, Kotani T, Kusakari S, Ohnishi H, Saito Y, et al. Promotion of cell spreading and migration by vascular endothelial-protein tyrosine phosphatase (VE-PTP) in cooperation with integrins. J Cell Physiol. 2010; 224:195–204. [PubMed: 20301196]
30. Gerhardt H, Golding M, Fruttiger M, Ruhrberg C, Lundkvist A, Abramsson A, et al. VEGF guides angiogenic sprouting utilizing endothelial tip cell filopodia. J Cell Biol. 2003; 161:1163–77. [PubMed: 12810700]
31. Krueger J, Liu D, Scholz K, Zimmer A, Shi Y, Klein C, et al. Flt1 acts as a negative regulator of tip cell formation and branching morphogenesis in the zebrafish embryo. Development. 2011; 138:2111–20. [PubMed: 21521739]
32. Ruhrberg C, Gerhardt H, Golding M, Watson R, Ioannidou S, Fujisawa H, et al. Spatially restricted patterning cues provided by heparin-binding VEGF-A control blood vessel branching morphogenesis. Genes Dev. 2002; 16:2684–98. [PubMed: 12381667]
33. Laise P, Di Patti F, Fanelli D, Masselli M, Arcangeli A. Deterministic and stochastic aspects of VEGF-A production and the cooperative behavior of tumoral cell colony. J Theor Biol. 2011; 272:55–63. [PubMed: 21167179]
34. Hubbell JA. Matrix-bound growth factors in tissue repair. Swiss Med Wkly. 2006; 136:387–91. [PubMed: 16847762]
35. Xie Y, Upton Z, Richards S, Rizzi SC, Leavesley DI. Hyaluronic acid: Evaluation as a potential delivery vehicle for vitronectin:growth factor complexes in wound healing applications. J Control Release. 2011 doi:10.1016/j.jconrel.2011.03.021.
36. Lei Y, Huang S, Sharif-Kashani P, Chen Y, Kavehpour P, Segura T. Incorporation of active DNA/cationic polymer polyplexes into hydrogel scaffolds. Biomaterials. 2010; 31:9106–16. [PubMed: 20822811]
37. Rayavarapu RG, Petersen W, Hartsuiker L, Chin P, Janssen H, van Leeuwen FW, et al. In vitro toxicity studies of polymer-coated gold nanorods. Nanotechnology. 2010; 21:145101. [PubMed: 20220222]

NIH-PA Author Manuscript

NIH-PA Author Manuscript

NIH-PA Author Manuscript

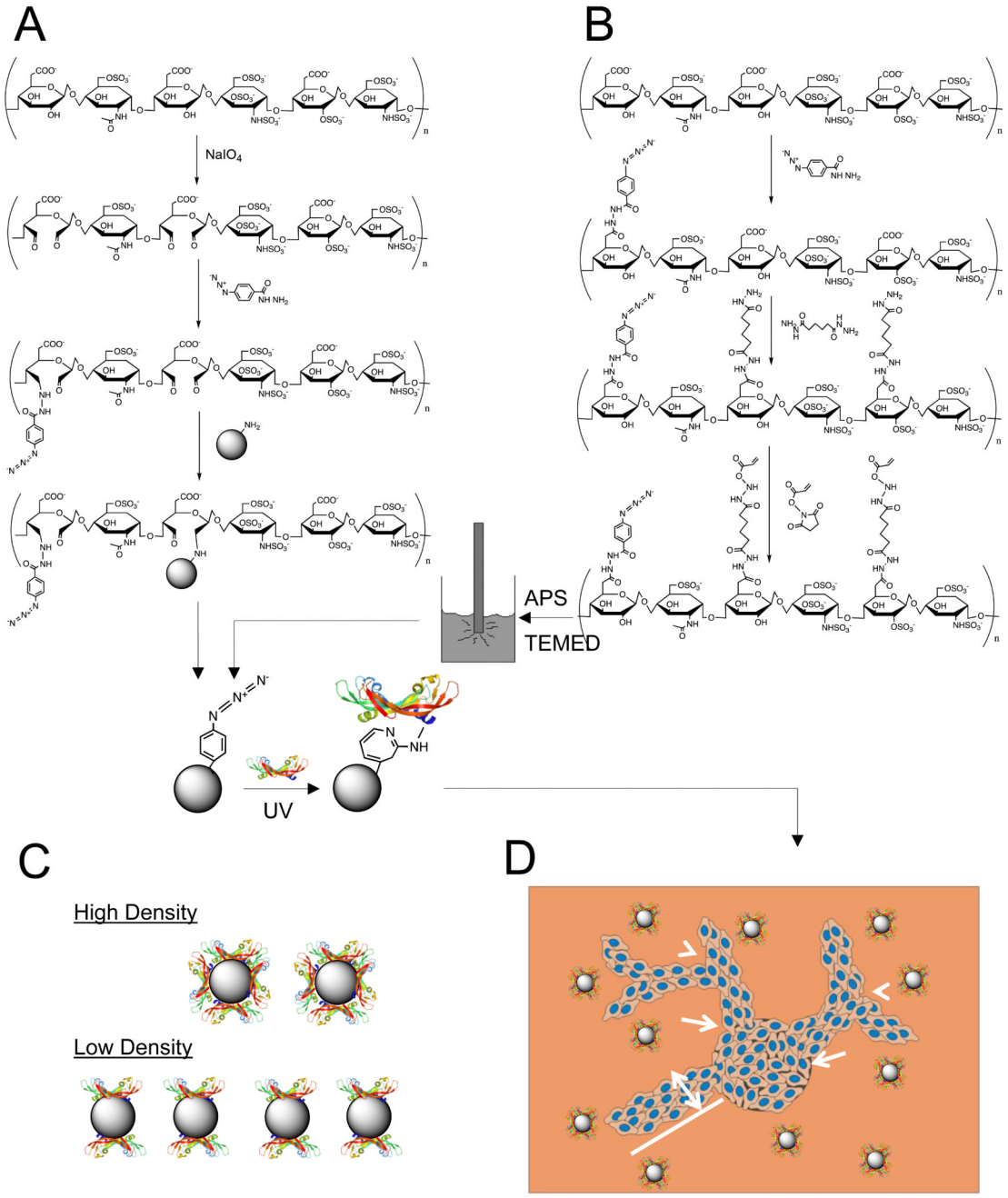

Figure 1.

VEGF modified particle synthesis. (A) Heparin coated polystyrene particles are fabricated by first oxidizing heparin to generate aldehyde groups. These groups are used to bind the photoactive crosslinker (ABH) and facilitate attachment to the amine-functionalized polystyrene particles. Once the particle is coated with heparin, the bind-and-lock strategy is employed. First VEGF interacts with heparin and forms its specific electrostatic interaction. Then, UV light activates the crosslinker, which non-specifically binds to the closest amine. The heparin-binding domain of VEGF has many available amines on the lysine groups that interact with the sulfate groups on heparin. (B) For the heparin nanoparticle, the heparin polymer chain is modified with the photoactive crosslinker and a dihydrazide through EDC

NIH-PA Author Manuscript

NIH-PA Author Manuscript

NIH-PA Author Manuscript

chemistry. The dihydrazide is reacted in a large enough molar ratio to saturate binding and avoid unwanted crosslinking. Once the modified polymer is purified, it is combined with surfactants into a hexane solution for sonication. During the inverse emulsion sonication process, radical initiators are added to the solution to generate radical polymerization. The formed nanoparticles are purified in a liquid-liquid extraction process and then bound to VEGF in a similar fashion as the heparin coated polystyrene particles. (C) High density and low density binding are utilized, where distribution of VEGF in the gel is varied by maintaining constant growth factor concentration with different number of particles. (D) With VEGF bound, the particles are introduced to a fibrin gel and analyzed for induction of branching (arrow heads) and sprouts (arrows) from endothelial cell-coated cytodex beads. Tube length (line) and tube thickness (double-headed arrow) are also quantified. Tube lengths are summed to give total network length.

NIH-PA Author Manuscript

NIH-PA Author Manuscript

NIH-PA Author Manuscript

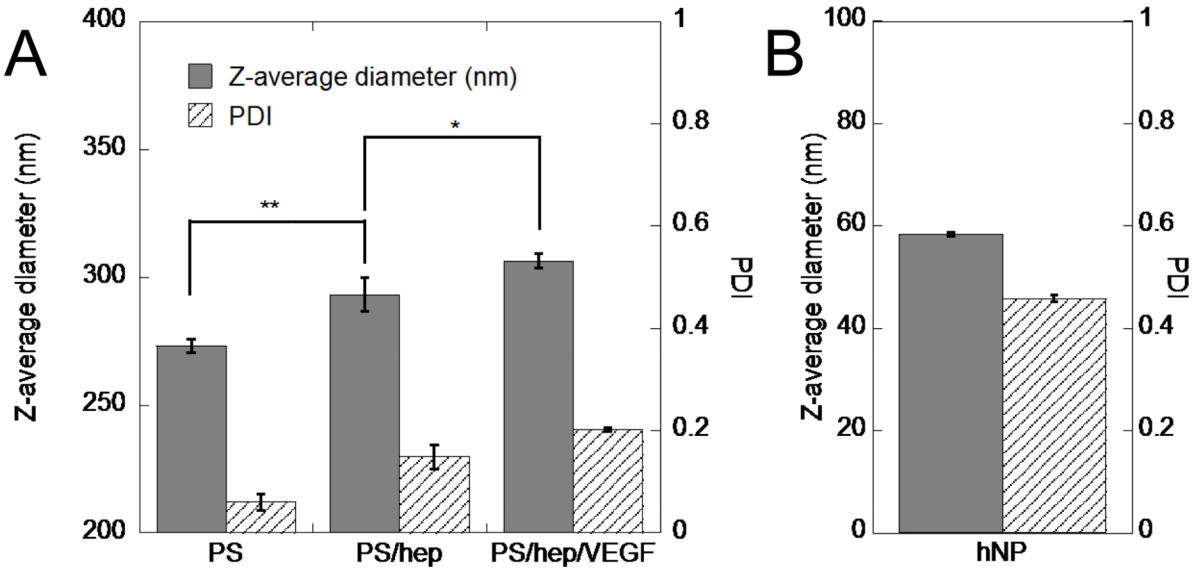

Figure 2.

Particle physical characterization. (A) DLS measurements of heparin-coated polystyrene nanoparticles show functionalization at each step. Each layer increases the diameter, but also the polydispersity, as expected. (B) DLS characterization of heparin nanoparticles shows a smaller average diameter than the polystyrene particles, but high polydispersity ($n = 3$, $*p < 0.05$, $**p < 0.01$).

NIH-PA Author Manuscript

NIH-PA Author Manuscript

NIH-PA Author Manuscript

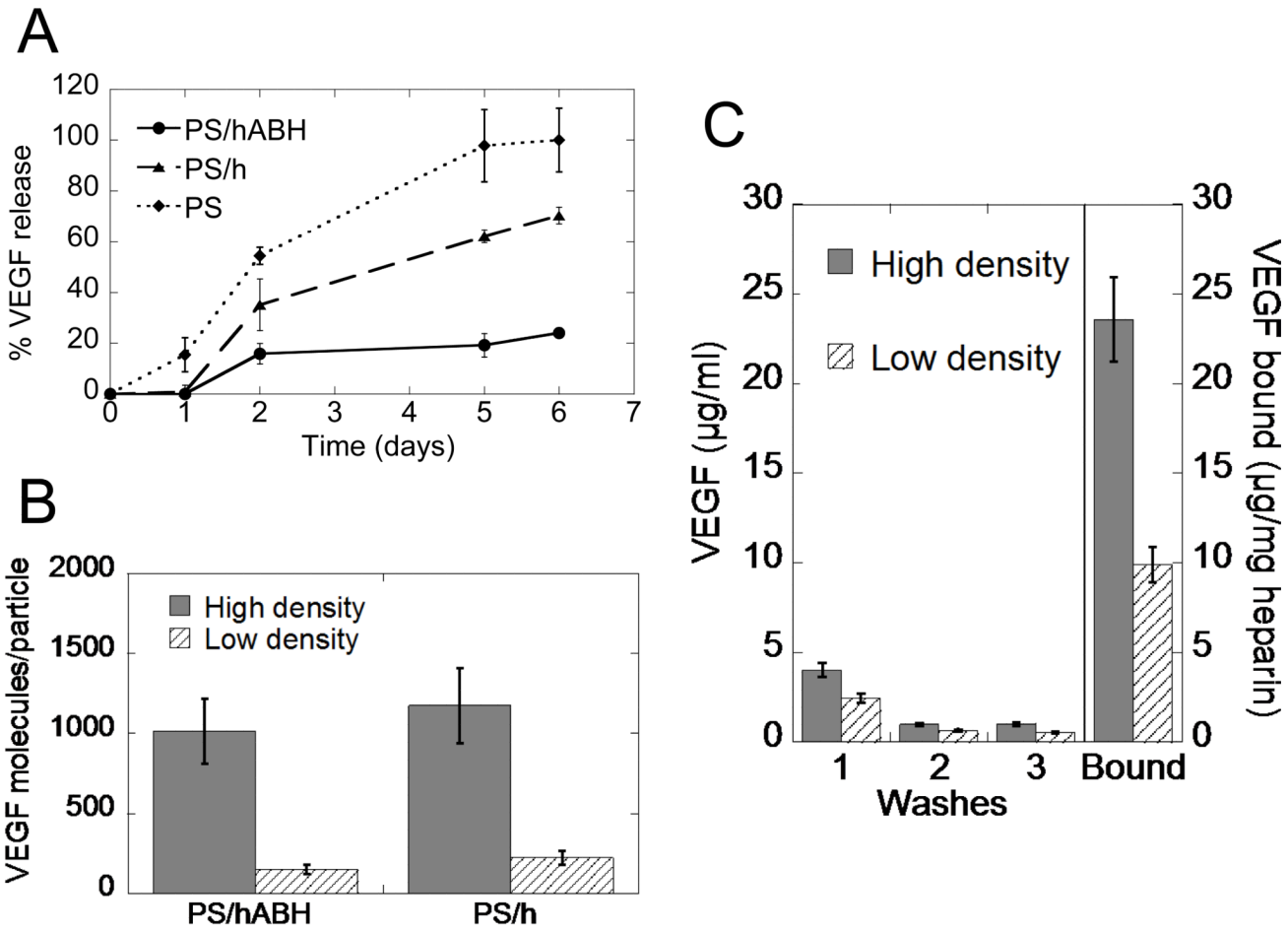

Figure 3.

Particle binding characterization. (A) Release profiles of heparin coated polystyrene particles in free heparin wash shows stability of VEGF covalent binding to particle. (B) Generation of high density and low density conditions for both particles with and without covalent binding indicates 1000 VEGF molecules/particle for high density condition, and 200 VEGF molecules/particle for low density condition. (C) VEGF is stably bound to heparin nanoparticles with different binding densities. Each successive wash has less VEGF until leveling (n = 3).

NIH-PA Author Manuscript

NIH-PA Author Manuscript

NIH-PA Author Manuscript

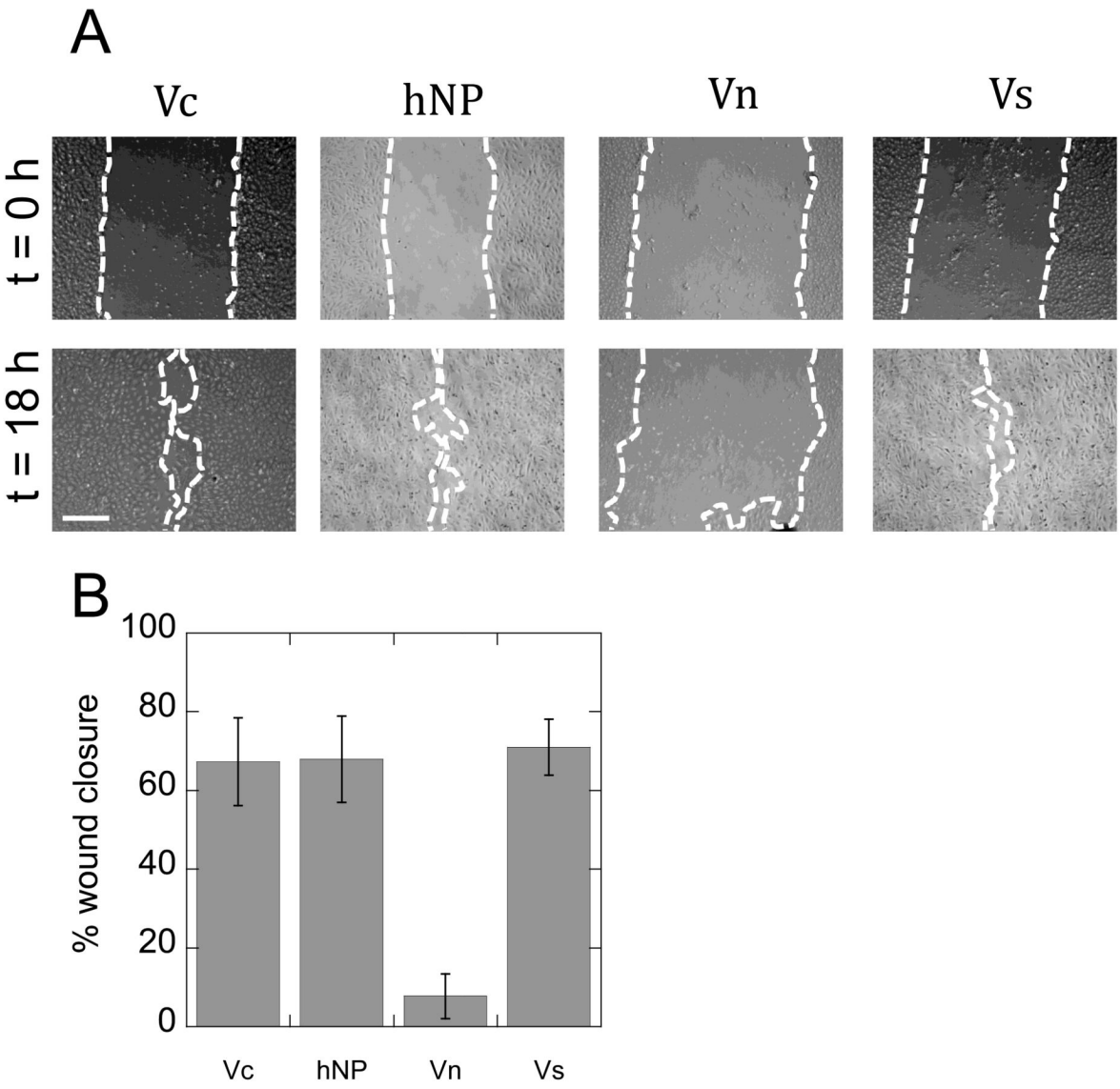

Figure 4.

Particle activity characterization. (A) Micrographs of cell migration experiment indicate movement of front from time 0 (top pictures) to 18 hours later (bottom pictures) in every condition except the negative control (Scale bar = 100 μm). (B) Quantification of the migration study shows particle bound VEGF is active. No statistical significance is observed between Vc, hNP, and Vs (n = 3).

NIH-PA Author Manuscript

NIH-PA Author Manuscript

NIH-PA Author Manuscript

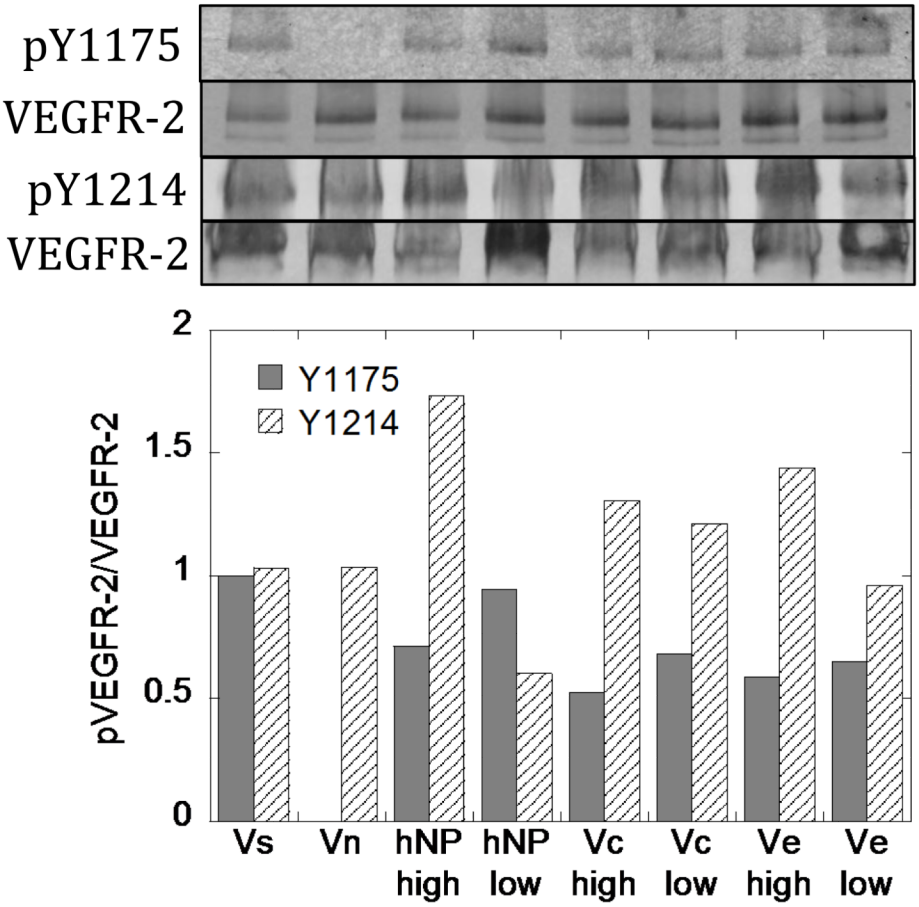

Figure 5.

VEGFR-2 phosphorylation assay. Binding of VEGF to particles enriches Y1214 signaling for all particles in all binding densities. Activation of Y1175 is slightly decreased. Each band has the blot intensity background subtracted from the band intensity, and then the intensity of the bands from the phospho- species are divided by the intensities from total VEGFR-2.

NIH-PA Author Manuscript

NIH-PA Author Manuscript

NIH-PA Author Manuscript

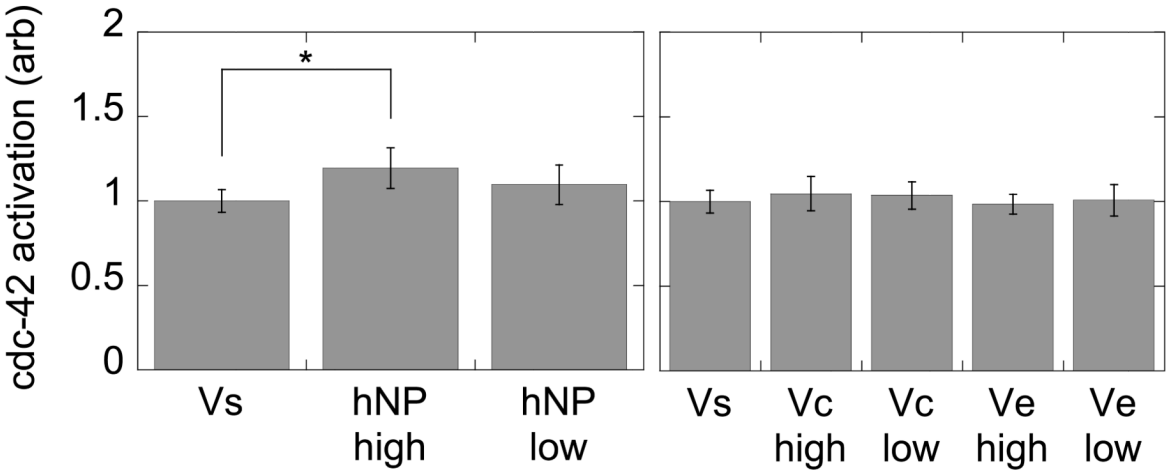

Figure 6.

cdc42 activation assay. Heparin nanoparticles with high density loading have a statistically significant increase in cdc42 activation over soluble VEGF. The polystyrene particles do no have a significant enhancement over the soluble condition (n = 5, *p < 0.05).

NIH-PA Author Manuscript

NIH-PA Author Manuscript

NIH-PA Author Manuscript

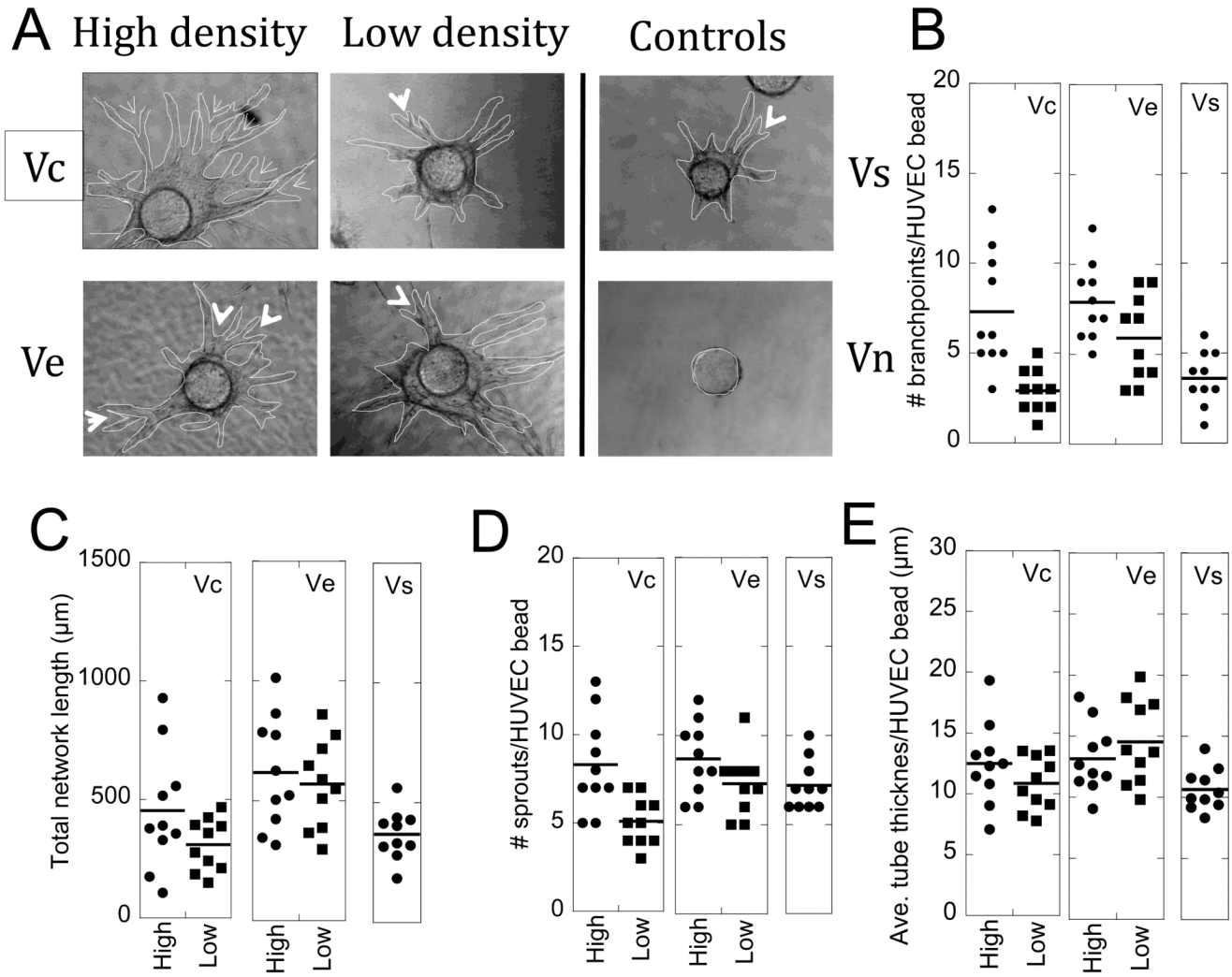

Figure 7.

Tube formation assay with polystyrene particles. (A) Phase micrographs of cytodex beads with endothelial cell sprouts after 9 days in culture. The endothelial tubes are outlined in red for clearer viewing. The arrow heads indicate branching points of tubes that sprout from the cytodex bead (Scale bar = 50 μm). (B) High density covalent binding leads to a significant increase in branching points for endothelial tubes (Vc high over Vc low (**$p < 0.01$), Vc high over soluble (**$p < 0.01$), Ve high over soluble (***$p < 0.001$)). The low density binding represents a more homogeneous distribution of the growth factor compared to high density binding. (C) Total network length quantification shows high density VEGF heparin nanoparticles lead to a significant increase in the size of the vessel network over Vs (***$p < 0.001$). (D) Quantification of the number of sprouts emanating from the cytodex beads is not statistically different between conditions. (E) Tube thickness also did not change significantly between the conditions. (n = 10).

NIH-PA Author Manuscript

NIH-PA Author Manuscript

NIH-PA Author Manuscript

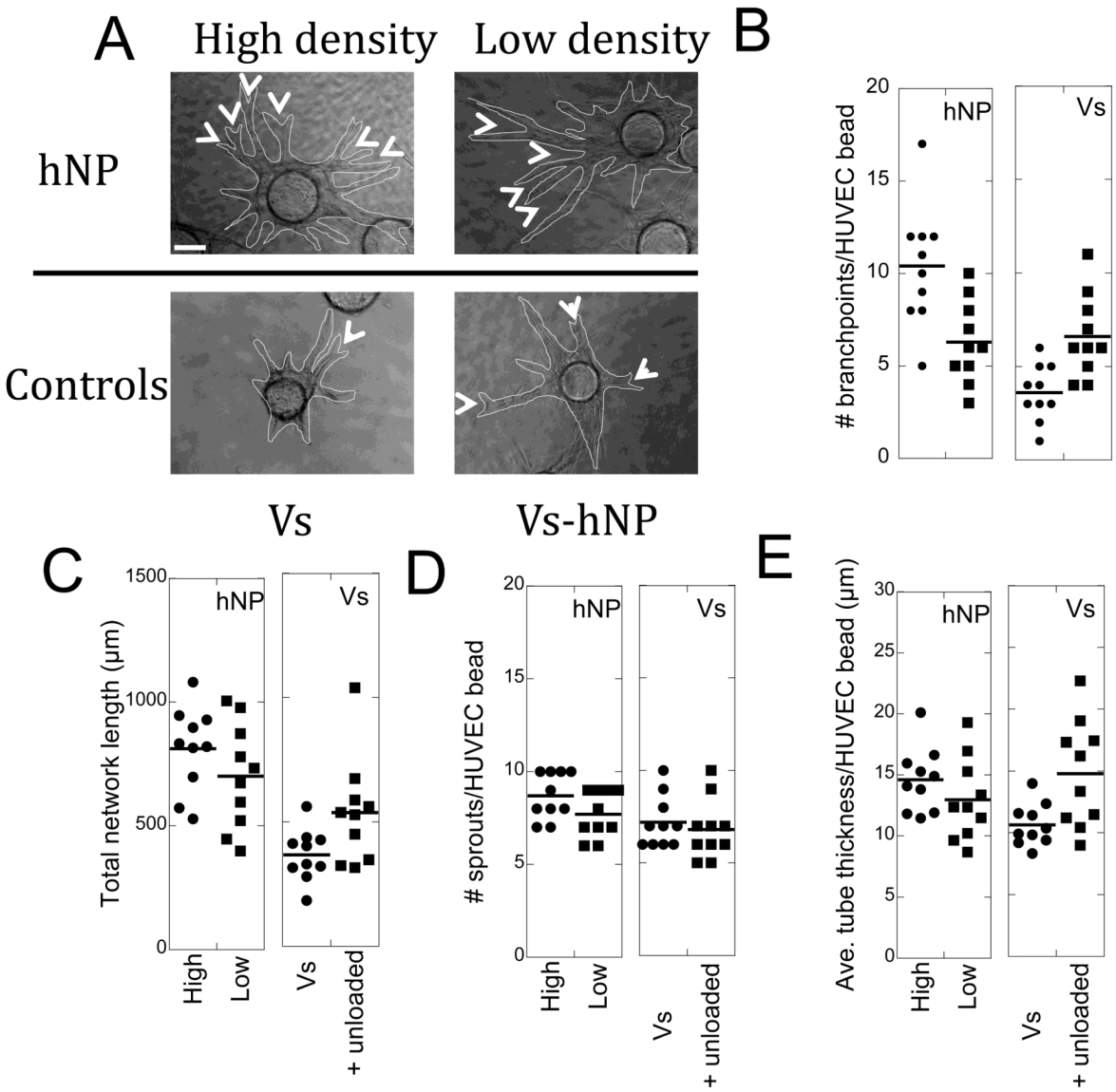

Figure 8.

Tube formation assay with heparin nanoparticles. (A) Phase micrographs of cytodex beads with endothelial cell sprouts after 9 days in culture. The endothelial tubes are outlined in red for clearer viewing. The arrow heads indicate branching points of tubes that sprout from the cytodex bead (Scale bar = 50 μm). (B) High density covalent binding leads to a significant increase in branching points for endothelial tubes (hNP high over hNP low (**$p < 0.01$), hNP high over soluble with (**$p < 0.01$) and without (***$p < 0.001$) unloaded hNP). Unloaded heparin nanoparticles refreshed with soluble VEGF showed a similar effect to the low density condition. The low density binding represents a more homogeneous distribution of the growth factor compared to high density binding. (C) Total network length quantification shows high density covalent VEGF heparin nanoparticles lead to a significant increase in the size of the vessel network (hNP high over Vs (***$p < 0.001$), over Vs-hNP (*$p < 0.05$); Vs-hNP over Vs (***$p < 0.001$)). (D) Quantification of the number of sprouts emanating from the cytodex beads is not statistically different between conditions. (E) hNP

high led to a significant increase in tube thickness over Vs (**$p < 0.01$), as did Vs-hNP (over Vs, **$p < 0.01$). ($n = 10$).

NIH-PA Author Manuscript
NIH-PA Author Manuscript
NIH-PA Author Manuscript

NIH-PA Author Manuscript

NIH-PA Author Manuscript

NIH-PA Author Manuscript

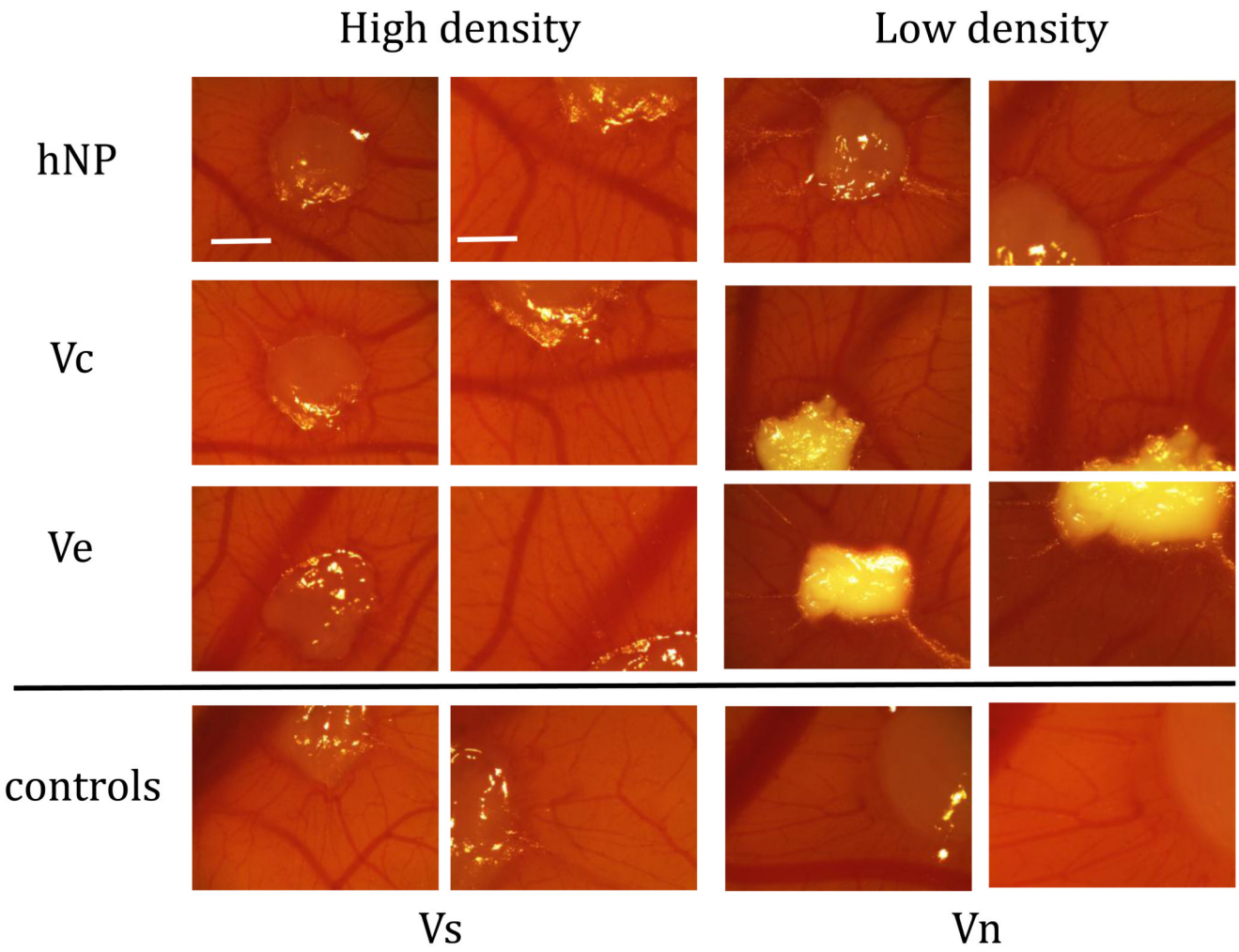

Figure 9.

CAM micrographs of fibrin implant and surrounding tissue show VEGF leads to induction of blood vessels surrounding implant. Since the low density conditions required more polystyrene particles, the fibrin gels became more opaque. The negative control, fibrin only (Vn), does not show the vascular induction of the other conditions with VEGF. Characteristic radial vessels originating from the implants are observed in every condition except the negative control (First and third column scale bar = 100 μm, second and fourth column scale bar = 60 μm).

NIH-PA Author Manuscript

NIH-PA Author Manuscript

NIH-PA Author Manuscript

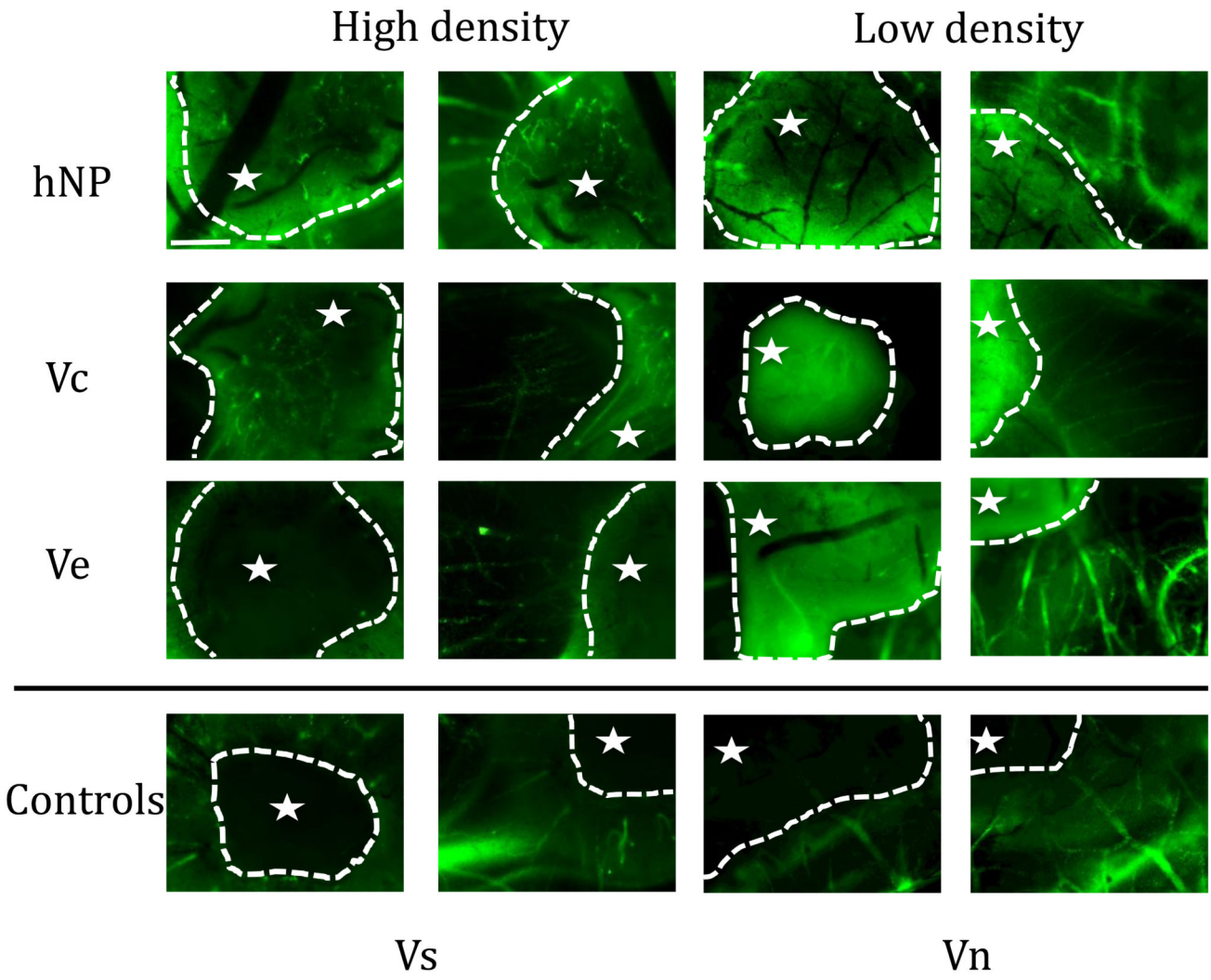

Figure 10.

CAM fluorescent micrographs of fibrin implant show that covalently bound VEGF leads to infiltration and branching of blood vessels within implant. Fluorescent micrographs were taken both of the implant itself and just outside the implant to show vessel morphology at the interface of the fibrin gel with the CAM (the star denotes the inside of the gel). Electrostatically bound VEGF releases and leads to radial vessel formation similar to the soluble VEGF condition (Scale bar = 25 μm).